

See discussions, stats, and author profiles for this publication at: <https://www.researchgate.net/publication/231654578>

Theoretical Analysis of the Performance of One-Dimensional Photonic Crystal-Based Dye-Sensitized Solar Cells

ARTICLE *in* THE JOURNAL OF PHYSICAL CHEMISTRY C · FEBRUARY 2010

Impact Factor: 4.77 · DOI: 10.1021/jp9096315

CITATIONS

48

READS

65

5 AUTHORS, INCLUDING:



[Gabriel Lozano](#)

Spanish National Research Council

49 PUBLICATIONS 579 CITATIONS

[SEE PROFILE](#)



[Ophélie Dematteo Caulier](#)

Université Bordeaux 1

20 PUBLICATIONS 63 CITATIONS

[SEE PROFILE](#)



[Mauricio E. Calvo](#)

Spanish National Research Council

55 PUBLICATIONS 720 CITATIONS

[SEE PROFILE](#)



[Hernán Míguez](#)

Spanish National Research Council

164 PUBLICATIONS 5,356 CITATIONS

[SEE PROFILE](#)

Theoretical Analysis of the Performance of One-Dimensional Photonic Crystal-Based Dye-Sensitized Solar Cells

Gabriel Lozano, Silvia Colodrero, Ophelie Caulier, Mauricio E. Calvo, and Hernán Míguez*

Instituto de Ciencia de Materiales de Sevilla, Consejo Superior de Investigaciones Científicas-Universidad de Sevilla, Américo Vespucio 49, 41092 Sevilla, Spain

Received: October 8, 2009; Revised Manuscript Received: January 18, 2010

A simple analytical model that allows designing one-dimensional photonic crystal based dye sensitized solar cells of optimized performance, accounting for the actual optical features of the device, is herein presented. Based on the theoretical description of the effect of coupling such Bragg mirrors to the light harvesting electrode, recently reported experimental values of the spectral dependence of incident photon to current conversion efficiency attained for such structures are fairly reproduced and rationalized. A thorough analysis of them in terms of the interplay between the effect of the electrode thickness and the characteristics of the Bragg reflection, such as intensity, spectral position, and width, is provided. Predictions on the maximum enhancement factors expected for realistic structures are also presented.

Introduction

The positive effect of coupling a photonic crystal to an absorbing electrode on power conversion efficiency has been demonstrated for a number of solar cells in the last years.^{1–7} The different physical mechanisms of enhancement have been thoroughly analyzed theoretically.^{8–10} Very recently, a significant increase of both light harvesting efficiency (LHE) and power conversion efficiency has been observed in dye-sensitized electrodes coupled to highly reflecting porous nanoparticle based one-dimensional photonic crystals (1DPCs), which act as coherent scattering layers.^{11,12} This approach, although not optimized yet, seeks to maximize the amount of light absorbed, while keeping some of the added values of the standard dye-sensitized solar cell, such as its semitransparency, which is lost when either a diffuse scattering layer or a metallic back mirror are used to enhance absorption. In this latter approach, besides, light must travel through a layer of absorbing electrolyte in which unproductive optical losses in terms of charge generation occur. On the other hand, 1DPCs are also capable of reflecting light of targeted wavelengths very intensely in spite of possessing a small thickness (around $0.5\text{ }\mu\text{m}$), so that no extra ohmic resistances that might cause a drop of the voltage are created. In fact, because the effect of the photonic crystal is similar to an increase of the photon flux, a rise of the open circuit photovoltage is expected,¹³ although it has not been observed yet. It has been experimentally shown that enhancement of optical absorption is due to both the partial localization of photons of certain narrow frequency ranges as well as to the increase of the optical path within the absorbing layer, which result from its coupling to the photonic crystal.¹² However, it is still lacking a theoretical description that allows devising actual 1DPC based solar cells, which must take into account the interplay between the effect of the working electrode thickness, the amount of dye absorbed, and the characteristics (spectral width and intensity) of the Bragg reflection resulting from the coupled photonic structure.

In this letter, we report on theoretical simulations of both the optical reflectance and the incident photon to current

conversion efficiency (IPCE) of porous one-dimensional photonic crystal-based dye-sensitized solar cells (DSSC). An analytical model that accounts for the actual optical features of the device is proposed. Its validity is confirmed by comparing its predictions with recently reported experimental values of the spectral dependence of the photogenerated current attained for such structures, which are fairly reproduced and rationalized. It is demonstrated that the interplay between the optical effect of the electrode thickness and the scattering strength of the photonic crystal determines the basic features of the performance of the cell and must be considered to design an optimized device. Predictions on the maximum enhancement factors expected for realistic structures are also presented.

Theoretical Model. Both the actual dye-sensitized electrode and the porous 1DPC are consecutively deposited onto a conducting fluorinated tin-oxide-coated transparent substrate. First, a layer of nanocrystalline titanium dioxide (TiO_2) particles was deposited onto a conducting transparent substrate by doctor blade, spin-coating, or a combination of both techniques. A coarse rough layer was attained through the former, but a uniform and smooth surface was achieved in the final coating after a drop of a suspension of fine TiO_2 particles was spun onto it. Then, to build the Bragg reflector onto this coated substrate, layers of SiO_2 and TiO_2 particles were deposited alternately by spin-coating so that a periodic modulation of the refractive index is built up in the direction perpendicular to the electrode surface. Optical interference effects occurring between the beams reflected and transmitted at the different interfaces created are at the origin of the photonic crystal properties of this type of periodic nanostructures. After performing the usual thermal annealing and sensitization processes, the cell is completed using a metal-covered counterelectrode and the internal space between the electrodes is filled with a liquid redox electrolyte that at the same time soaks the porous photonic crystal, thus yielding electrical contact between the different parts of the cell. This ensemble is herein modeled through a layered structure, as depicted in Figure 1, in which the notation used in the simulation to represent the thickness and refractive index of each relevant slab is included. The incoming and outgoing media are considered to be the upper and lower glass

* Corresponding author. E-mail: hernan@icmse.csic.es.

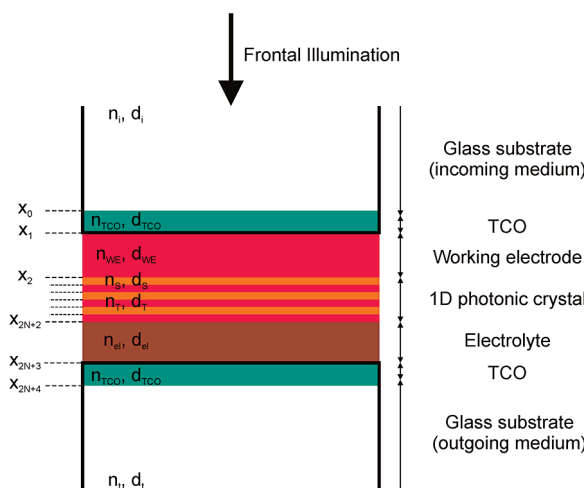


Figure 1. Scheme of a DSSC coupled to a 1DPC showing the illumination through the dye-coated TiO_2 layer (frontal illumination).

substrates, respectively. This is done to prevent the appearance of very short period ($<1 \text{ nm}$) fringes arising from the presence of thick ($>5 \text{ mm}$) entrance and exit plane parallel slabs, which largely make difficult the analysis of the relevant optical data. This effect is illustrated and analyzed in the Supporting Information. Such ripples are usually not detectable experimentally since they are blurred by the lack of homogeneity of the

substrate thickness at the few nanometres length scale. In our model, we also take into account the optical effects due to the presence of the transparent conducting oxide coating, whose thickness and refractive index are d_{TCO} and n_{TCO} , respectively. The dyed nanocrystalline slab that acts as the cell working electrode presents as relevant parameters its thickness, d_{WE} , and its complex refractive index, n_{WE} , given by the expression:

$$n_{\text{WE}} = n_{\text{TiO}_2} + \beta(\lambda)i \quad (1)$$

The real part of the refractive index, n_{TiO_2} , is determined by the refractive index of the TiO_2 nanocrystals and the liquid electrolyte filling the pore space between them. We assume that the imaginary part of the refractive index of the working electrode is mainly determined by the ruthenium dye because its molar absorption coefficient in the spectral region of interest is between 1 and 2 orders of magnitude larger than that of the electrolyte,¹⁴ and their concentration in the electrode is similar.¹⁵ This allows us to establish a direct relation between the absorptance of the cell and the light harvesting efficiency that contributes effectively to the photocurrent. The frequency-dependent imaginary part of the refractive index of the dyed nc- TiO_2 layer used in the calculations is:

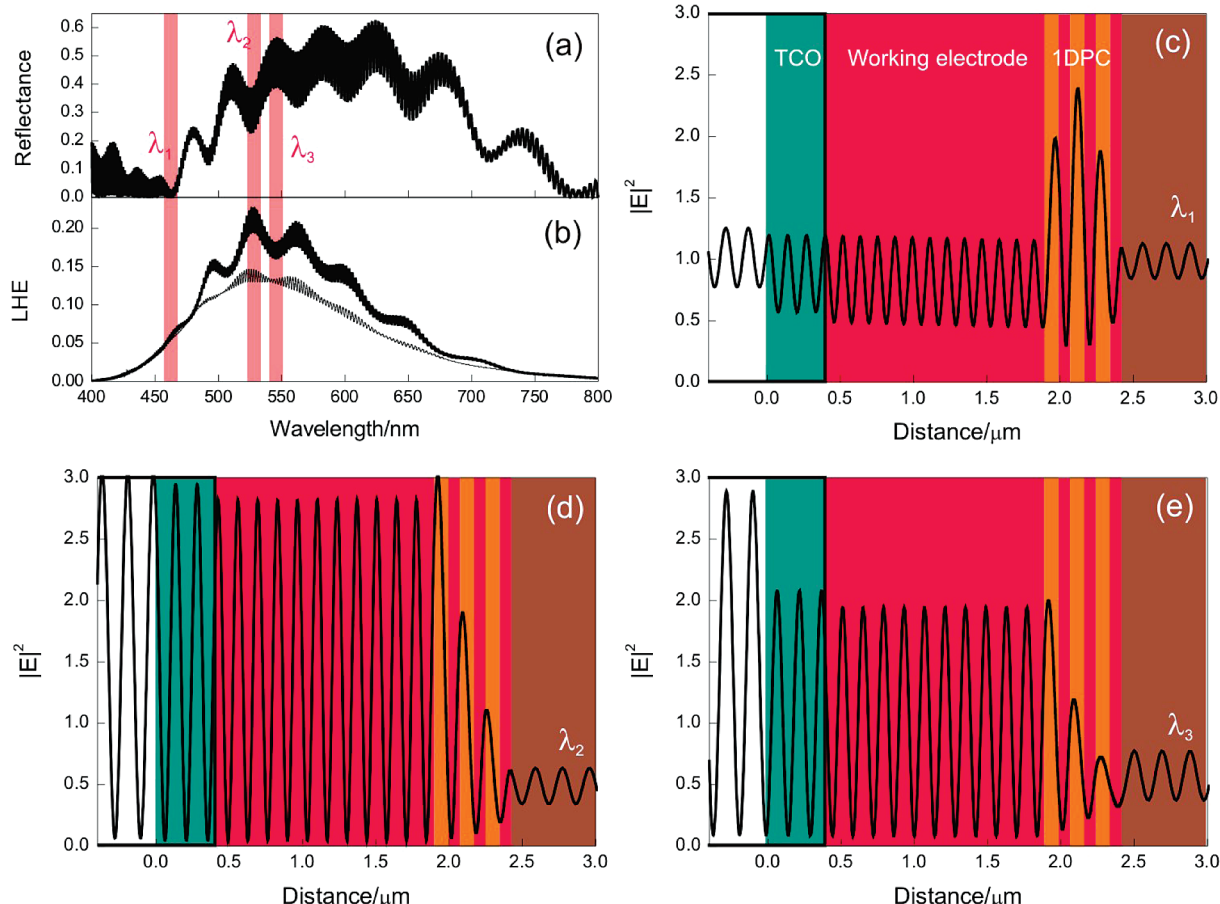


Figure 2. Reflectance (a) and light harvesting efficiency (LHE) spectra (b) for a DSSC containing a 1DPC (three unit cells) coupled to a dye-sensitized nc- TiO_2 layer of $1.5 \mu\text{m}$. For comparison, we plot the LHE for the same electrode without the photonic crystal. (c–e) Spatial distribution of the square amplitude of the electric field of the system described in (a) at three selected wavelengths: (c) $\lambda_1 = 463 \text{ nm}$; (d) $\lambda_2 = 528 \text{ nm}$; and (e) $\lambda_3 = 545 \text{ nm}$. Parameters employed for this simulations are $n_{\text{TCO}} = 1.80$, $d_{\text{TCO}} = 400 \text{ nm}$, $d_{\text{WE}} = 1.5 \mu\text{m}$, $n_{\text{TiO}_2} = 1.95$, $\beta_0 = 0.004$, $n_s = 1.43$, $d_s = 95 \text{ nm}$, $n_t = 1.92$, $d_t = 80 \text{ nm}$, $n_{\text{el}} = 1.433$, and $d_{\text{el}} = 50 \mu\text{m}$.

$$\beta(\lambda) = \beta_0 \exp(1 - z(\lambda) - e^{-z(\lambda)}), \quad \text{with}$$

$$z(\lambda) = \frac{\lambda - \lambda_0}{\Delta\lambda} \quad (2)$$

which is the result of fitting the photocurrent and absorptance data reported for similar electrodes in the literature.^{1,8} Please notice that β_0 can be related to the amount of dye adsorbed onto the titanium dioxide nanocrystals, whereas $z(\lambda)$ depends on the specific sensitizer dye employed; in our case, for a ruthenium bipyridyl complex, $\lambda_0 = 538$ nm, and $\Delta\lambda = 64.16$ nm. Thus, different dye loads of the electrode can be simulated through variations of β_0 .

The rest of slabs forming the modeled cell, that is, the nanoparticle SiO_2 and TiO_2 films the photonic crystal is made of, and the space filled by the electrolyte are characterized by their respective thickness and refractive index, namely, (d_S, n_S) , (d_T, n_T) , and (d_{el}, n_{el}) . Thus, the porous nanoparticle based photonic crystal is simulated by the alternate stack of several slabs characterized by the parameters (d_S, n_S) and (d_T, n_T) . A unit cell is formed by one pair of these slabs. In our case, we have simulated the effect of photonic crystals whose thickness ranges from $N = 3$ to $N = 10$, where N is the number of unit cells. Both n_S and n_T are estimated considering that the pores of the SiO_2 and TiO_2 layers, respectively, are fully filled by the electrolyte solution.

Our theoretical model should serve, in the first place, to describe the optical reflectance (R) and incident photon to current conversion efficiency (IPCE) values that have been reported in refs 11 and 12. As in those experiments, in our simulation the incoming radiation impinges perpendicularly to the working electrode (frontal illumination conditions) and therefore to the stacking of dielectric layers. The electric field is treated as a scalar rather than a vector wave and it is considered to depend on just one spatial variable (x). Such simplified scalar wave approximation (SWA) have proven to provide a good description of the optical response of photonic crystals for specific directions and at low energy ranges,¹⁶ as it is actually the case under study here.

To attain the R and the IPCE, it is necessary to calculate the reflection and transmission coefficients of the fields in the incident and outgoing media, labeled as r and t , respectively. Because partially transmitted and reflected waves are generated at each interface present in the multilayer, the expressions for the electric field in each one of the slabs is

$$E(x) = \begin{cases} e^{ikx} + re^{-ikx}, & -\infty \leq x \leq x_0 \\ C_1 e^{ik_{TCO}x} + C_2 e^{-ik_{TCO}x}, & x_0 \leq x \leq x_1 \\ C_3 e^{ik_{WE}x} + C_4 e^{-ik_{WE}x}, & x_1 \leq x \leq x_2 \\ C_5 e^{ik_{S}x} + C_6 e^{-ik_{S}x}, & x_2 \leq x \leq x_3 \\ \vdots & \vdots \\ C_{4N+3} e^{ik_{T}x} + C_{4N+4} e^{-ik_{T}x}, & x_{2N+1} \leq x \leq x_{2N+2} \\ C_{4N+5} e^{ik_{el}x} + C_{4N+6} e^{-ik_{el}x}, & x_{2N+2} \leq x \leq x_{2N+3} \\ C_{4N+7} e^{ik_{TCO}x} + C_{4N+8} e^{-ik_{TCO}x}, & x_{2N+3} \leq x \leq x_{2N+4} \\ te^{ikx}, & x_{2N+4} \leq x \leq \infty \end{cases} \quad (3)$$

with

$$\begin{aligned} x_0 &= 0 \\ x_1 &= d_{TCO} \\ x_2 &= d_{TCO} + d_{WE} \\ x_3 &= d_{TCO} + d_{WE} + d_S \\ &\vdots \\ x_{2N+1} &= d_{TCO} + d_{WE} + Nd_S + (N-1)d_T \\ x_{2N+2} &= d_{TCO} + d_{WE} + N(d_S + d_T) \\ x_{2N+3} &= d_{TCO} + d_{WE} + N(d_S + d_T) + d_{el} \\ x_{2N+4} &= d_{TCO} + d_{WE} + N(d_S + d_T) + d_{el} + d_{TCO} \end{aligned}$$

where k_i , k_{TCO} , k_{WE} , k_S , k_T , k_{el} , and k_t are the wavevectors in the homogeneous incident medium, the transparent conducting oxide coating, the working electrode, the silica and titania layers forming the photonic crystal (PC), the electrolyte, and the outgoing media, respectively. Please notice that, except for the final transmission medium, in all the rest of the slabs considered, the electric field is taken to be the sum of a propagating and a counter-propagating wave, with similar wavevectors but opposite direction and amplitude, given by the coefficients labeled, generically, as C_j . Please notice that the wavevector is given by the general expression:¹⁷

$$k_j(\lambda) = \frac{2\pi n_j(\lambda)}{\lambda} \quad (4)$$

in which the refractive index may be complex and frequency dependent.

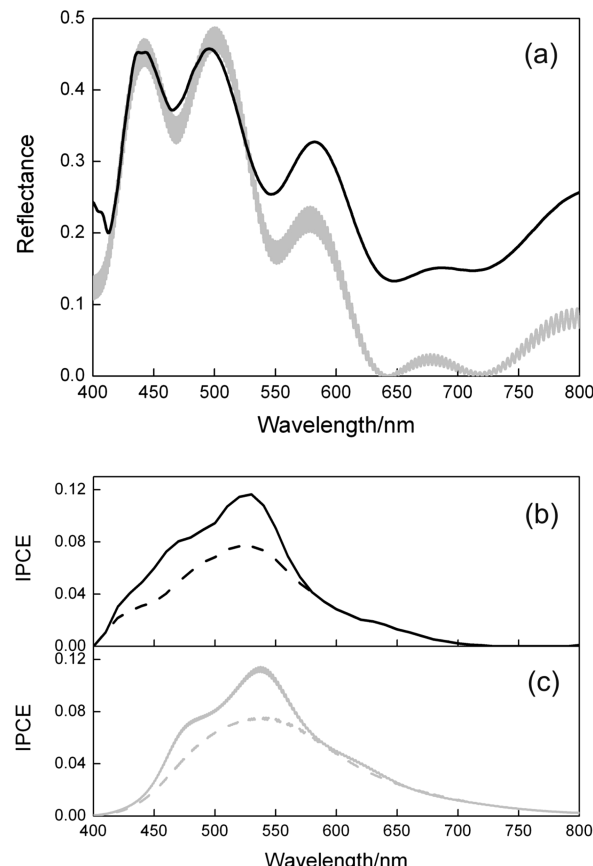


Figure 3. (a) Experimental (black line) and theoretical (gray line) specular reflectance spectra for a cell containing a 1DPC coupled to a 600 nm thick dyed TiO_2 electrode. Experimental (b) and theoretical (c) IPCE curves for the cell above-mentioned (solid lines). For comparison, IPCE curves for a reference cell are also plotted (dashed lines).

The frequency-dependent coefficients r , t , and C_j are determined by imposing continuity conditions for both the electric field and its first derivative across the interface from one medium to the next. This establishes a set of equations that we solve by making use of the transfer matrix formalism. This method allows determining only the coefficients relevant for each particular case (in this case, r and t), thus, largely reducing the computation time and permitting us to test a large number of structures. Under this formalism, the set of equations can be expressed:

$$\begin{aligned}
 & \underbrace{\begin{pmatrix} e^{ik_i x_0} & e^{-ik_i x_0} \\ ik_i x_0 e^{ik_i x_0} & -ik_i x_0 e^{-ik_i x_0} \end{pmatrix}}_{M_{x_0}^i} \begin{pmatrix} 1 \\ r \end{pmatrix} = \underbrace{\begin{pmatrix} e^{ik_{TCO} x_0} & e^{-ik_{TCO} x_0} \\ ik_{TCO} x_0 e^{ik_{TCO} x_0} & -ik_{TCO} x_0 e^{-ik_{TCO} x_0} \end{pmatrix}}_{M_{x_0}^f} \begin{pmatrix} C_1 \\ C_2 \end{pmatrix} \\
 & \underbrace{\begin{pmatrix} e^{ik_{TCO} x_1} & e^{-ik_{TCO} x_1} \\ ik_{TCO} x_1 e^{ik_{TCO} x_1} & -ik_{TCO} x_1 e^{-ik_{TCO} x_1} \end{pmatrix}}_{M_{x_1}^i} \begin{pmatrix} C_1 \\ C_2 \end{pmatrix} = \underbrace{\begin{pmatrix} e^{ik_{WE} x_1} & e^{-ik_{WE} x_1} \\ ik_{WE} x_1 e^{ik_{WE} x_1} & -ik_{WE} x_1 e^{-ik_{WE} x_1} \end{pmatrix}}_{M_{x_1}^f} \begin{pmatrix} C_3 \\ C_4 \end{pmatrix} \\
 & \underbrace{\begin{pmatrix} e^{ik_{WE} x_2} & e^{-ik_{WE} x_2} \\ ik_{WE} x_2 e^{ik_{WE} x_2} & -ik_{WE} x_2 e^{-ik_{WE} x_2} \end{pmatrix}}_{M_{x_2}^i} \begin{pmatrix} C_3 \\ C_4 \end{pmatrix} = \underbrace{\begin{pmatrix} e^{ik_S x_2} & e^{-ik_S x_2} \\ ik_S x_2 e^{ik_S x_2} & -ik_S x_2 e^{-ik_S x_2} \end{pmatrix}}_{M_{x_2}^f} \begin{pmatrix} C_5 \\ C_6 \end{pmatrix} \\
 & \underbrace{\begin{pmatrix} e^{ik_S x_3} & e^{-ik_S x_3} \\ ik_S x_3 e^{ik_S x_3} & -ik_S x_3 e^{-ik_S x_3} \end{pmatrix}}_{M_{x_3}^i} \begin{pmatrix} C_5 \\ C_6 \end{pmatrix} = \underbrace{\begin{pmatrix} e^{ik_T x_3} & e^{-ik_T x_3} \\ ik_T x_3 e^{ik_T x_3} & -ik_T x_3 e^{-ik_T x_3} \end{pmatrix}}_{M_{x_3}^f} \begin{pmatrix} C_7 \\ C_8 \end{pmatrix} \\
 & \vdots \\
 & \underbrace{\begin{pmatrix} e^{ik_{el} x_{2N+2}} & e^{-ik_{el} x_{2N+2}} \\ ik_{el} x_{2N+2} e^{ik_{el} x_{2N+2}} & -ik_{el} x_{2N+2} e^{-ik_{el} x_{2N+2}} \end{pmatrix}}_{M_{x_{2N+2}}^i} \begin{pmatrix} C_{4N+3} \\ C_{4N+4} \end{pmatrix} = \underbrace{\begin{pmatrix} e^{ik_{el} x_{2N+2}} & e^{-ik_{el} x_{2N+2}} \\ ik_{el} x_{2N+2} e^{ik_{el} x_{2N+2}} & -ik_{el} x_{2N+2} e^{-ik_{el} x_{2N+2}} \end{pmatrix}}_{M_{x_{2N+2}}^f} \begin{pmatrix} C_{4N+5} \\ C_{4N+6} \end{pmatrix} \\
 & \underbrace{\begin{pmatrix} e^{ik_{el} x_{2N+3}} & e^{-ik_{el} x_{2N+3}} \\ ik_{el} x_{2N+3} e^{ik_{el} x_{2N+3}} & -ik_{el} x_{2N+3} e^{-ik_{el} x_{2N+3}} \end{pmatrix}}_{M_{x_{2N+3}}^i} \begin{pmatrix} C_{4N+5} \\ C_{4N+6} \end{pmatrix} = \underbrace{\begin{pmatrix} e^{ik_{TCO} x_{2N+3}} & e^{-ik_{TCO} x_{2N+3}} \\ ik_{TCO} x_{2N+3} e^{ik_{TCO} x_{2N+3}} & -ik_{TCO} x_{2N+3} e^{-ik_{TCO} x_{2N+3}} \end{pmatrix}}_{M_{x_{2N+3}}^f} \begin{pmatrix} C_{4N+7} \\ C_{4N+8} \end{pmatrix} \\
 & \underbrace{\begin{pmatrix} e^{ik_{TCO} x_{2N+4}} & e^{-ik_{TCO} x_{2N+4}} \\ ik_{TCO} x_{2N+4} e^{ik_{TCO} x_{2N+4}} & -ik_{TCO} x_{2N+4} e^{-ik_{TCO} x_{2N+4}} \end{pmatrix}}_{M_{x_{2N+4}}^i} \begin{pmatrix} C_{4N+7} \\ C_{4N+8} \end{pmatrix} = \underbrace{\begin{pmatrix} e^{ik_T x_{2N+4}} & e^{-ik_T x_{2N+4}} \\ ik_T x_{2N+4} e^{ik_T x_{2N+4}} & -ik_T x_{2N+4} e^{-ik_T x_{2N+4}} \end{pmatrix}}_{M_{x_{2N+4}}^f} \begin{pmatrix} t \\ 0 \end{pmatrix}
 \end{aligned}$$

If the electric field is known at the beginning of a layer, the field at the end of the same layer can be derived from a simple matrix operation. A stack of layers can then be represented as a system matrix, which is the product of the individual matrices corresponding to each intermediate slab considered within the system. In this way, it can be directly obtained the relation between reflection (r) and transmission (t) coefficients of the fields in the incident and outgoing media:

$$\begin{aligned}
 \begin{pmatrix} 1 \\ r \end{pmatrix} &= M \begin{pmatrix} t \\ 0 \end{pmatrix} = [M_{x_0}^i]^{-1} M_{x_0}^f [M_{x_1}^i]^{-1} M_{x_1}^f [M_{x_2}^i]^{-1} M_{x_2}^f \cdots \\
 [M_{x_{2N+3}}^i]^{-1} M_{x_{2N+3}}^f [M_{x_{2N+4}}^i]^{-1} M_{x_{2N+4}}^f \begin{pmatrix} t \\ 0 \end{pmatrix} &= \begin{pmatrix} m_{11} & m_{12} \\ m_{21} & m_{22} \end{pmatrix} \begin{pmatrix} t \\ 0 \end{pmatrix} \quad (6)
 \end{aligned}$$

Therefore, reflectance (R) and transmittance (T) are determined using the following relations:¹⁷

$$\begin{aligned}
 R &= |r|^2 = \left| \frac{m_{21}}{m_{11}} \right|^2 \\
 T &= \frac{n_t}{n_i} |t|^2 = \frac{n_t}{n_i} \left| \frac{1}{m_{11}} \right|^2
 \end{aligned} \quad (7)$$

Finally, the light harvesting efficiency (LHE) or absorptance (A) is obtained by employing the well-known equation

$$LHE = A = 1 - R - T \quad (8)$$

The relation between the LHE of a dye-sensitized solar cell and the IPCE is given by¹⁸

$$IPCE(\lambda) = \Phi(\lambda) \xi(\lambda) LHE(\lambda) \quad (9)$$

where $\Phi(\lambda)$ is the electron-transfer yield and $\xi(\lambda)$ is the charge collecting efficiency by the glass supported electrode. The integral of this expression weighted by the solar radiation spectrum yields the photogenerated short circuit current density J_{SC} :

$$J_{SC} = \int q IPCE(\lambda) F(\lambda) d\lambda \quad (10)$$

where q is the electron charge and $F(\lambda)$ is the ratio between the solar spectral irradiance and the photon energy. The increment of photocurrent density (ΔJ_{SC}) attained when a 1DPC is coupled to a dyed nc-TiO₂ electrode is defined as follows:

$$\Delta J_{SC} = \frac{\int q\Phi(\lambda)\xi(\lambda)LHE_{PC}(\lambda)F(\lambda)d\lambda - \int q\Phi(\lambda)\xi(\lambda)LHE_{ref}(\lambda)F(\lambda)d\lambda}{\int q\Phi(\lambda)\xi(\lambda)LHE_{ref}(\lambda)F(\lambda)d\lambda} \quad (11)$$

where LHE_{PC} is the LHE of a DSSC coupled to a 1DPC, whereas LHE_{ref} refers to that of a DSSC used as reference. For our calculations we use a simplified version of eq 11 in which both $\Phi(\lambda)$ and $\xi(\lambda)$ are assumed to be constant and equal to 1.

The model herein proposed allows also calculating the stationary fields within the layered structure under analysis, which helps to visualize the effect of integrating the photonic crystal on the actual spatial distribution of the radiation in the cell. In Figure 2a,b, we compare the simulated reflectance spectrum of a PC-based DSSC and its LHE with those of a reference cell. It can be clearly seen the correspondence between spectral peaks of absorptance and dips in reflectance, which are the fingerprint of optical resonant modes localized in the film coupled to the PC. It is important to point out that as the thickness of the dye-sensitized electrode increases, the number of localized modes rises and so does the number of peaks in the LHE curve. We have also calculated the spatial distribution of the squared magnitude of the electric field for three selected frequencies impinging under front-illumination conditions (please see Figure 2c–e). These are chosen to illustrate the origin of the spectral response of the PC-based cell. For the sake of clarity, we have neglected the imaginary part of the refractive index of the dye, so the localization effects of the electric field can be better appreciated. It can be clearly seen that at the spectral position where one of the dips in reflectance attributed to a resonant mode is found (λ_2), localization is stronger within the electrode than that observed for frequencies outside the band gap (λ_1) or at one of the reflectance peaks (λ_3). The field intensity within the electrode for those frequencies lying within band gap frequencies but not affected by localization (λ_3) is also increased as a result of being back-reflected by the 1DPC. Hence, although less efficient, it constitutes a second enhancement mechanism provided by the 1DPC, as it was mentioned before.

Results and Discussion

To check the suitability of the proposed theoretical model, we use eqs 7 and 11 to calculate the R and the IPCE of 1DPC-based cells similar to those previously studied experimentally in refs 11 and 12. In both cases, three unit cell photonic crystals were implemented. Figure 3 shows the simulated (gray solid line) and experimental (black solid line) specular reflectance and IPCE curves for a cell containing a SiO_2 – TiO_2 nanoparticle-based 1DPC coupled to a 600 nm thick electrode made of dyed titanium dioxide nanocrystallites, as reported in ref 12. For comparison, experimental and calculated data of the IPCE curves obtained from a reference dye-sensitized TiO_2 electrode of the same thickness but with no photonic crystal coupled are also plotted (dashed black and gray lines) in Figure 3b and c, respectively. Good agreement between simulated and experimental reflectance spectra measured under frontal illumination conditions is obtained, as displayed in Figure 3a, with both the shape and the intensity of the experimental optical features being reproduced by the theoretical curve. This agreement evidences the high optical quality of the nanoparticle-based 1DPCs, because the fittings can be performed without considering the effect of diffuse scattering. Dips in the reflectance spectrum of the cell indicate the presence of modes partially localized within

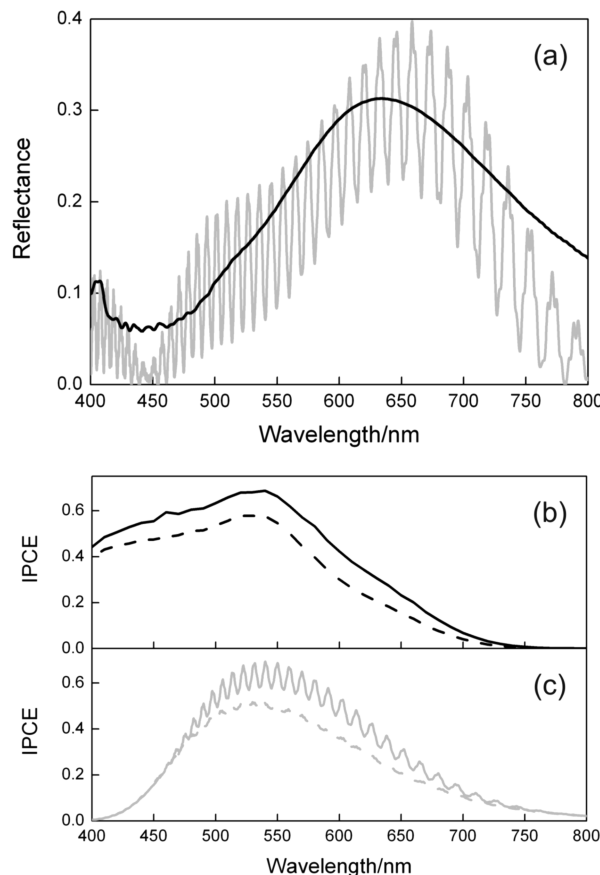


Figure 4. (a) Experimental (black line) and theoretical (gray line) specular reflectance spectra for a cell containing a 1DPC coupled to a 7.5 μm thick dyed TiO_2 electrode. Experimental (b) and theoretical (c) IPCE curves for the cell above-mentioned (solid lines). For comparison, IPCE curves for a reference cell are also plotted (dashed lines).

the working electrode.¹⁶ The values of the fitting parameters defined in the previous section are, in this case, $n_{\text{TiO}_2} = 1.92$, $\beta_0 = 0.0055$, $n_s = 1.43$, and $n_T = 1.88$.¹⁹ The lattice parameter of the periodic stack has been estimated to be 140 nm ($d_s = 60$ nm, $d_T = 80$ nm). Please note that the amount of absorbing material for the reference and the 1DPC-based cell is the same, which we simulate by keeping constant both the thickness and the imaginary part (β_0) of the refractive index of the layer that simulates the light absorbing electrode. In this case, and for the rest of the calculations performed, we assume a layer of electrolyte of refractive index $n_{\text{el}} = 1.43$ and thickness $d_{\text{el}} = 50$ μm , although it was found that the results were basically independent of d_{el} for thicknesses above 10 μm . Considering these parameters, the different IPCE curves attained for the reference and the PC-based solar cell are fairly reproduced by the simulations, as clearly shown in Figure 3b,c. The photocurrent enhancement is larger at the spectral regions at which photons are partially localized within the working electrode due to the effect of the coupling to the 1DPC.

A similar analysis was carried out for the case of a DSSC having the same periodic structure based on SiO_2 – TiO_2 nanoparticles coupled to a 7.5 μm thick dye-sensitized electrode, as those reported in ref 11. In Figure 4, we show the simulated (solid gray line) and the experimental (solid black line) specular reflectance, as well as the incident photon to current conversion efficiency (IPCE), for this solar cell. For comparison, we also plot the IPCE curves, experimental and theoretical, obtained for a reference cell in Figure 4b and c (dashed black and gray lines). As in the previous case, a clear agreement between

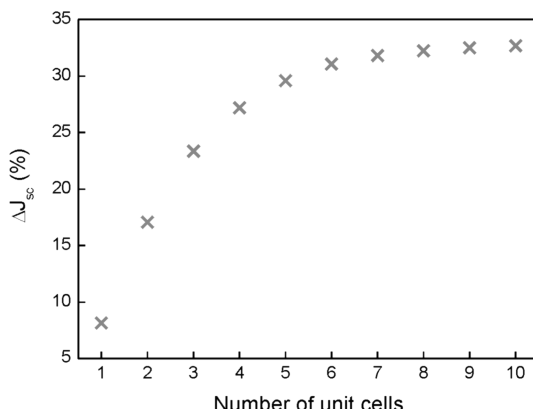


Figure 5. Increment of photogenerated current vs the number of layers that constitute the PC structure coupled to a $7.5\ \mu\text{m}$ thick absorbing electrode. The lattice parameter has been considered to be constant for all cases.

simulated and experimental reflectance spectra and IPCE curves is observed. The simulated optical response and IPCE show multiple optical resonance modes, which is a consequence of coupling a photonic crystal to a much thicker electrode, thus, creating multiple resonant frequencies partially localized within the absorbing electrode. These resonances are not easy to distinguish experimentally because they are blurred by the slight variations of the electrode thickness. In this case, the lattice parameter of the 1DPC has been estimated to be 175 nm ($d_s = 95\ \text{nm}$, $d_t = 80\ \text{nm}$) and the values of the fitting parameters are now $n_{\text{TiO}_2} = 1.95$, $\beta_0 = 0.004$, $n_s = 1.43$, and $n_t = 1.92$. Please notice that the value of the parameter β_0 , which we relate to the amount of dye adsorbed on the crystallites, is slightly smaller in this latter case. This has been confirmed experimentally by performing desorption experiments on the actual cells following a reported procedure.²⁰

Once confirmed, the validity of the model proposed by contrasting it with previous experimental results, we analyze the effect of coupling 1DPCs having a different number of unit cells (N). This strongly determines the photonic strength of the lattice, that is, the intensity and width of the Bragg peak. We then calculate ΔJ_{sc} using eq 11 for periodic stacks having $d_s = 95\ \text{nm}$, $d_t = 80\ \text{nm}$, $n_s = 1.43$, and $n_t = 1.92$ and coupled to an electrode characterized by $d_{\text{WE}} = 7.5\ \mu\text{m}$ and $\beta_0 = 0.004$, that is, similar values to those used to fit the results reported in ref 11, but in this case, the number of unit cells is varied between $N = 1$ and $N = 10$. Because the Bragg reflection intensity increases with the number of layers, the performance of the device is also expected to increase. In Figure 5, we plot the value of the ΔJ_{sc} predicted versus the number of unit cells forming the 1DPC. It can be seen that ΔJ_{sc} increases rapidly with the number of layers present in thin stacks. However, for $N > 5$, ΔJ_{sc} tends asymptotically to a stationary value ($\approx 35\%$), which indicates that the reflectance of the multilayer infiltrated with the electrolyte is close to one. Please notice that the actual reflectance of the whole ensemble will not be one, because absorption of the electrode will strongly modify this value. These results indicate that optimization of the DSSC is possible with the techniques that have been developed to build this type of porous 1DPC up to date because they allow depositing up to $N = 10$ unit cells. In the experimental data reported in ref 11 in which the 1DPC used was made of three unit cells, a 25% increment in the short circuit photocurrent was observed for an optimized 1DPC-based DSSC operating under 1 sun illumination, very close to the theoretical ones presented in Figure 5. However, the enhancement of power conversion efficiency was

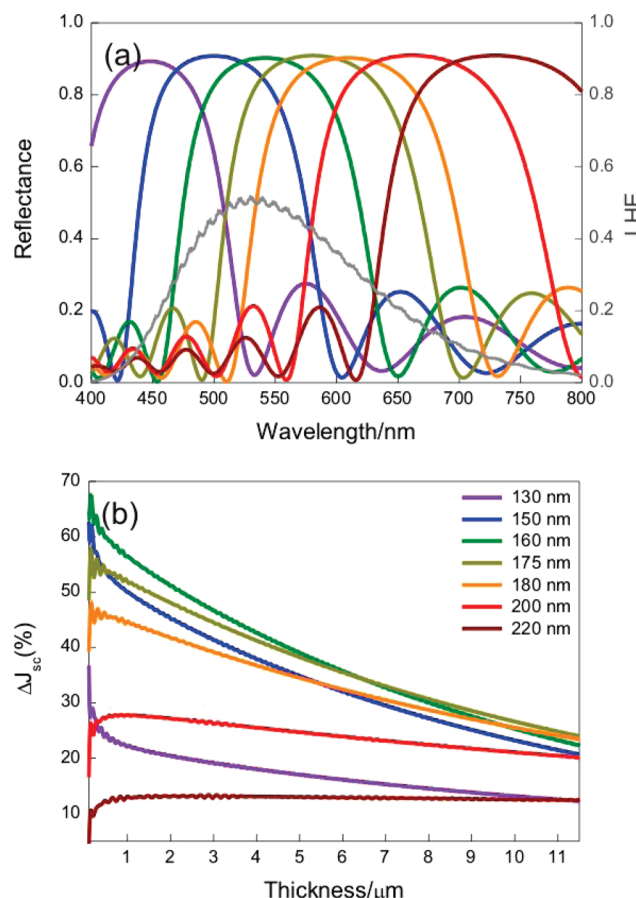


Figure 6. (a) Calculated specular reflectance for a 14 layer 1DPC with different lattice parameters: 130 nm ($d_s = 60\ \text{nm}$, $d_t = 70\ \text{nm}$; violet line), 150 nm ($d_s = 80\ \text{nm}$, $d_t = 70\ \text{nm}$; blue line), 160 nm ($d_s = 80\ \text{nm}$, $d_t = 80\ \text{nm}$; green line), 175 nm ($d_s = 95\ \text{nm}$, $d_t = 80\ \text{nm}$; dark yellow), 180 nm ($d_s = 90\ \text{nm}$, $d_t = 90\ \text{nm}$; orange line), 200 nm ($d_s = 110\ \text{nm}$, $d_t = 90\ \text{nm}$; red line), and 220 nm ($d_s = 120\ \text{nm}$, $d_t = 100\ \text{nm}$; brown line). Calculated LHE (gray line) for a reference electrode for which we have considered $\beta_0 = 0.004$. (b) Calculated increment of photogenerated current for dye-sensitized electrodes having different thicknesses coupled to the 1DPC shown in (a) for the same value of β_0 . Graph legend attached indicates the values of the 1DPC lattice parameters.

experimentally found to be a 15%. This difference may be explained by the lower fill factor attained when using a photonic crystal as scattering layer, which indicates that charge transport is hindered by the presence of the multilayer. This comparison clearly shows that there is still room for improvement in the application of porous 1DPC in DSSC. Further developments may come from the optimization of the diffusion of the electrolyte through the pore network of the optical lattice. Besides, any resistance potentially introduced by the photonic crystal will have a larger effect at higher illumination conditions because its effect increases with the number of carriers. If this is the case, hence, a reduction of the incident radiation intensity will improve the relative performance of the cell, as it was actually reported in ref 11.

Finally, we chose 7 unit cells thick 1DPCs as scattering layers to analyze the interplay between the position of the Bragg reflection and the electrode thickness (d_{WE}). For such a multilayer, the maximum light harvesting enhancement effect is almost achieved. To change the spectral position of the primary reflectance peak, we vary the lattice parameter between 130 and 220 nm, using at the same time different values of the pair (d_s , d_t), as indicated in the caption of Figure 6. By doing so, the

peak sweeps the whole visible spectrum. To give it more generality, we have used different values of β_0 ($\beta_0 = 0.004$, $\beta_0 = 0.0055$, and $\beta_0 = 0.008$) to simulate three degrees of loading of the dye in the structure, although all results shown in Figure 6 correspond to $\beta_0 = 0.004$. In Figure 6a, we plot the calculated absorptance spectrum (LHE) corresponding to a $7.5 \mu\text{m}$ thick dyed electrode using such β_0 (gray line). The results attained for the rest of β_0 are included as Supporting Information. Superimposed, we draw the simulated reflectance of 1D periodic structures with different lattice parameter (color lines) to show explicitly the degree of overlap between the spectral regions in which high optical scattering and absorption occur. The ΔJ_{sc} attained for working electrodes of diverse d_{WE} coupled to the 1DPCs, whose Bragg reflections are plotted in Figure 6a, are shown in Figure 6b. It can be seen that the magnitude of the photocurrent enhancement effect caused by the coupling to the 1DPC lowers as the thickness of the electrode increases, because more photons are absorbed by the dyed nc-TiO₂ layer when they first pass through it. Consequently, the effect of increasing the amount of absorbing material (β_0) is also to reduce the enhancement factor due to the presence of the 1DPC (please see Supporting Information). For thin electrodes, the highest enhancement factors are attained coupling 1DPCs whose Bragg peak overlaps most of the absorption band of the ruthenium dye. For thick electrodes, this trend changes and red reflecting 1DPCs are found to perform better because the ruthenium dye less effectively captures solar radiation precisely for $\lambda > 600 \text{ nm}$. Thus, once the rest of parameters (d_{WE} , β_0) have been optimized, it is in this spectral region where light harvesting must be more strongly enhanced to improve conversion efficiency. At the view of these curves, we can conclude that for standard electrodes of 7 to $8 \mu\text{m}$ we can realistically expect enhancements of the photocurrent of 35% for optimized samples. Because the power conversion efficiency is directly proportional to the short circuit photocurrent, similar enhancements may be expected for the overall performance of the cell as long as the rest of the parameters of the device are not altered by the presence of the photonic crystal. For electrodes of thicknesses smaller than $3 \mu\text{m}$, enhancements between 50 and 70% are expected. These values, although very significant, are much lower than those reported in ref 12 for the enhancement of the power conversion efficiency of thin electrodes, which were of even a few hundred percent. Our calculations thus indicate that such a difference cannot be entirely attributed to optical effects.

Conclusions

We have developed a simple analytical model that accurately describes the enhancement effect on incident photon to current conversion efficiency of a one-dimensional photonic crystal coupled to a dye-sensitized electrode. By considering the realistic optical features of the device, recently reported experiments can be fairly reproduced and rationalized within this approach. The interplay between the effect of the electrode thickness and the position, width, and intensity of the Bragg optical reflection has been understood and shown to be critical

to optimize the device. Predictions on the maximum enhancement factors expected for realistic structures have also been presented.

Acknowledgment. This work has been funded by the company NLAB Solar, the Spanish Ministry of Science and Education under Grant MAT2008-02166, Junta de Andalucía under Grant FQM3579, and Project HOPE (Consolider-Ingenio 2010) CSD2007-00007. G.L. and M.C. thank the Spanish Research Council for funding of their scholarships and contracts under the JAE program.

Supporting Information Available: Calculated specular reflectance spectra for a 1DPC based DSSC in which the upper and lower glass substrates are considered finite and semi-infinite respectively (Figure S1), and calculated increment of photo-generated current for dye-sensitized electrodes having different thicknesses coupled to the 1DPC for $\beta_0 = 0.0055$ and $\beta_0 = 0.008$ (Figure S2). This material is available free of charge via the Internet at <http://pubs.acs.org>.

References and Notes

- Nishimura, S.; Abrams, V.; Lewis, B. A.; Halaoui, L.; Mallouk, T. E.; Benkstein, K. D.; Lagemaat, J.; Frank, A. J. *J. Am. Chem. Soc.* **2003**, *125*, 6306.
- O'Brien, P.; Kherani, N. P.; Zukotynski, S.; Ozin, G. A.; Vekris, E.; Tetreault, N.; Chutinan, A.; John, S.; Mihi, A.; Míguez, H. *Adv. Mater.* **2007**, *19*, 4177.
- Mihi, A.; Calvo, M. E.; Anta, J. A.; Míguez, H. *J. Phys. Chem. C* **2008**, *112*, 13.
- Ko, D. H.; Tumbleston, J. R.; Zhang, L.; Williams, S.; DeSimone, J. M.; Lopez, R.; Samulski, E. T. *Nano Lett.* **2009**, *9*, 2742.
- Prieto, I.; Galiana, B.; Postigo, P. A.; Algara, C.; Martínez, L. J.; Rey-Stolle, I. *Appl. Phys. Lett.* **2009**, *94*, 191102.
- Chang, T. H.; Wu, P. H.; Chen, S. H.; Chan, C. H.; Lee, C. C.; Chen, C. C.; Su, Y. K. *Opt. Express* **2009**, *17*, 6519.
- Zeng, L.; Yi, Y.; Hong, C.; Liu, J.; Feng, N.; Duan, X.; Kimerling, L. C.; Alamaru, B. A. *Appl. Phys. Lett.* **2006**, *89*, 111111.
- Mihi, A.; Míguez, H. *J. Phys. Chem. B* **2005**, *109*, 15968.
- Bermel, P.; Luo, C.; Zeng, L.; Kimerling, L. C.; Joannopoulos, J. D. *Opt. Express* **2007**, *15*, 16986.
- Tumbleston, J. R.; Ko, D. H.; Samulski, E. T.; Lopez, R. *Appl. Phys. Lett.* **2009**, *94*, 043305.
- Colodrero, S.; Mihi, A.; Häggman, L.; Ocaña, M.; Boschloo, G.; Hagfeldt, A.; Míguez, H. *Adv. Mater.* **2009**, *21*, 764.
- Colodrero, S.; Mihi, A.; Anta, J. A.; Ocaña, M.; Míguez, H. *J. Phys. Chem. C* **2009**, *113*, 1150.
- Nelson, J. *The Physics of Solar Cells*; Imperial College Press: London, 2003, ISBN 1860943403.
- Awtrey, A. D.; Connick, R. E. *J. Am. Chem. Soc.* **1951**, *73*, 1842.
- Grätzel, M. *Inorg. Chem.* **2005**, *44*, 6841.
- Mihi, A.; Míguez, H.; Rodríguez, I.; Rubio, S.; Meseguer, F. *Phys. Rev. B* **2005**, *71*, 125131.
- Hecht, E.; Zajac, A. *Optics* Addison-Wesley Iberoamericana: Argentina, 1986; ISBN 0201028395.
- Tachibana, Y.; Hara, K.; Sayama, K.; Arakawa, H. *Chem. Mater.* **2002**, *14*, 2527.
- We assume that the refractive indices of the titania and silica particles are 2.44 and 1.43, respectively; the final values of n_T and n_S attained for the layers they form from the fittings are in good agreement with the expected results of averaging the refractive index of the nanoparticles and that of the interstitial volume filled with electrolyte using Bruggeman equation.
- Nakade, S.; Matsuda, M.; Kambe, S.; Saito, Y.; Kitamura, T.; Sakata, T.; Wada, Y.; Mori, H.; Yanagida, S. *J. Phys. Chem. B* **2002**, *106*, 10004.